

Numerical Prediction of Heat Transfer and Fluid Flow Characteristics in a Circular Microchannel with Bifurcation Plate

Valaparla Ranjith Kumar

Department of Mechanical Engineering,
National Institute of Technology, Warangal, 506004 Telangana, India
Corresponding author: valaparlaranjith@gmail.com

Karthik Balasubramanian

Department of Mechanical Engineering,
National Institute of Technology, Warangal, 506004, Telangana, India

K. Kiran Kumar

Department of Mechanical Engineering
National Institute of Technology, Warangal, 506004. Telangana, India

(Received December 25, 2018; Accepted August 28, 2019)

Abstract

Hydrothermal characteristics in circular wavy microchannels (CWMCs) with bifurcation plate have been numerically studied and compared with hydrothermal performance of sinusoidal wavy microchannels (SWMCs). Numerical study were carried out considering the Reynolds number (Re) ranging from 100 to 300. It was observed that, as the fluid flows through CWMC, it continuously absorbs heat from the channel leading to decrease in the temperature difference between the channel and the fluid. Hence, heat dissipation along the channel length decreases. To augment the heat dissipation along the fluid flow direction in CWMC, bifurcation plate (BFP) is introduced in the middle of the channel. CWMC with bifurcation plate has shown higher Nusselt number (Nu) with pressure drop penalty. The parametric study on bifurcation plate length was also carried out to minimize the pressure drop penalty and to achieve higher Nu. It is identified that CWMC with bifurcation plate length of 12.5 mm gives higher Nu with pressure drop penalty. Nu is further enhanced by providing slots on bifurcation plate. It is concluded that CWMC with BFP(10 mm) having slots gives the highest Nu than any other designs with pressure drop penalty.

Keywords- Circular wavy microchannel, Bifurcation plate, Bifurcation plate with slots, Dean vortices.

1. Introduction

As day to day growth of technology and modernization of electronic devices, several conventional heat dissipation technologies have not been able to meet the desired cooling effect. Effective heat dissipation from these devices plays a vital role in the operational functioning of these devices. To dissipate huge heat from compact electronic devices a novel heat dissipation technology i.e. microchannels (MCs) heat sink cooling technology was first introduced and established by Tuckerman and Pease in 1981 (Tuckerman and Pease, 1981). Kandlikar and Grande (2004) in their review studied various cooling technologies (air cooling, water cooling) that have been adopted to cool the high heat flux integrated circuit chips. They discussed its merits, demerits, fouling considerations, manufacturing technologies and cost. They also discussed the need for microchannels and performance enhancement techniques such as microstructures within the channels and walls. Karathanassis et al. (2013) numerically studied the hydrothermal characteristics of MCs in which changing the channel width in stepwise. They concluded that, their proposed MCs geometry shows superior heat transfer and lower pressure drop compared to uniform width MCs.

Xie et al. (2015) studied the hydrothermal characteristics of straight MCs with integrated internal vertical Y-shaped bifurcation plates having different lengths and different angles of the arms. They concluded that 25 mm internally Y-shaped bifurcation plate with MCs shown superior heat dissipation with the same pumping power than other geometries. They also observed that in their introduced geometry with an arm angle of 180° have 10% lower thermal resistance than other geometries considered, with the same pumping power.

Knight et al. (1992); Ambatipudi and Rahman (2000) studied the significance of channel aspect ratio, number of channels and Re on hydrothermal characteristics of straight microchannels. They concluded that higher Nu at more number of channels, optimum channel depth ($300\mu\text{m}$) at Re equal to 673. Liu and Garimella (2004) studied the heat transfer characteristics in straight microchannels in the Re range 300 to 3500 with channel width varied in the range $194\mu\text{m}$ to $534\mu\text{m}$ at a depth five times normal width. They concluded that wide mismatches occurred between the conventional correlation and experimental values and numerical results are aligned with a deviation of 5%. Hasan et al. (2009) studied the significance of channel cross section on hydrothermal characteristics. They concluded that microchannels with circular cross section shown superior overall performance and second one is square cross section among the other cross section (Rectangular, Iso-triangular and Trapezoidal).

Sui et al. (2010) numerically investigated hydrothermal characteristics in wavy MCs by changing the relative wave length in flow direction. They concluded that wavy MCs shown higher Nu than straight MCs with lesser pressure drop penalty. They also concluded enhancement in Nu predominant than pressure drop penalty. Chiam et al. (2016) numerically studied the hydrothermal characteristics of wavy microchannels with 45° branched secondary channels. They also studied overall performance factor of their introduced design at full amplitude and half amplitude. They concluded that wavy microchannel with 45° branched secondary channel with half amplitude showed higher overall performance factor than full amplitude in the Re range considered in their study. Kumar et al. (2019) numerically studied hydrothermal characteristics in sinusoidal wavy MCs with tangential branched secondary channels in the Re range 100 to 300. They concluded that sinusoidal wavy MCs with tangential branched secondary channels at optimum secondary channel width 0.15mm shown superior overall performance (23%) than sinusoidal wavy MCs with 45° branched secondary channels at secondary channel width 0.3mm . Kumar et al. (2018) numerically studied hydrothermal characteristics in circular wavy MCs in the Re range 100 to 300. They concluded that, their proposed design has same channel radius of curvature between the crest and trough, where as its varied in case of sinusoidal wavy MCs. It provided stronger Dean vortices and subsequently higher Nu with smaller pressure drop penalty. Dean and Hurst (1959) first made a speculative estimates that Dean vortices development were initiated by centrifugal instability while the fluid flows through curved channels and concluded that centrifugal instability occurs across the channel width and this leads to Dean vortices formation across the channel width.

Based the above literature survey on various numerical and experimental studies, it is observed that in wavy microchannel, Dean vortices strength varies from crest to trough. Also, as the fluid flows from the inlet to outlet in the microchannel, the temperature difference between the fluid and channel is decreased. This leads to drop in heat transfer rate in micro channels. To address these issues, CWMC, CWMC with bifurcation plate (BFP) and CWMC with BFP with slots are introduced and compared their hydrothermal characteristics with SWMC. 3-D steady state numerical study was carried out in the Re range of 100 to 300 with uniform heat flux (50 W/cm^2) wall boundary conditions.

Nomenclature

A	Wave amplitude (m)	MC	Microchannels
A_b	Channel base area (m ²)	Nu	Nusselt number
A_w	Channel inner wall surface area (m ²)	p_i	Inlet pressure (Pa)
BFP	Bifurcation plate	p_o	Outlet pressure (Pa)
CWMC	Circular wavy microchannel	Pr	Prandtl number
De	Dean Number	q''	Heat flux (W/m ²)
D_h	Hydraulic diameter (m)	Re	Reynolds number
f	Friction factor	S	Channel substrate (solid) thickness (m)
H	Channel height (m)	SWMC	Sinusoidal wavy microchannel
h	Convective heat transfer coefficient (W/m ² K)	T	Temperature (K)
k	Thermal conductivity (W/m. K)	u, v, w	Velocity components in X,Y and Z--direction
L	Wavelength (m)	W	channel width (m)

Greek Symbols

μ	Dynamic viscosity (kg/m.s)	ρ	Density (kg/m ³)
-------	----------------------------	--------	------------------------------

Subscripts

avg.	average	o	outlet
b	base	s	Solid
f	Fluid	w	wall
h	hydraulic	x	local
i	inlet		

2. Microchannel Model and Mathematical Formulation

Figure 1 shows the CWMC with a sectional view and CWMC with bifurcation plate which were used in current study. Solid and fluid domains in geometry are created in SOLIDWORKS modelling software by using the equation $y = A \cos(2\pi x/L)$ and in CWMC where fluid domain is created by the circular profile for the total length of the heat sink. The created model is imported into ANSYS fluent and meshing of the computational domains is done in ANSYS Mesh. Channel substrate height and width are taken as 1.2 mm and 0.6 mm whereas half of these dimensions are considered as channel passage dimensions. In CWMC with bifurcation plate (BFP), a thin fin with a thickness and height of 0.1 mm and 0.6 mm respectively is introduced in the middle of the channel. Bifurcation plate length from the outlet varies from 7.5 mm to 12.5 mm with steps of 2.5 mm.

The continuity, momentum and energy equations are solved to analyze the hydrothermal characteristics of wavy microchannel (MC) by considering the following assumptions:

- (i) Laminar fluid flow.
- (ii) Steady state heat transfer.
- (iii) Working fluid is incompressible
- (iv) Thermophysical properties of working fluid and channel material are not dependent on temperature, except the dynamic viscosity of fluid.
- (v) MC heatsink fin tips are adiabatic in nature
- (vi) Uniform heat flux is applied at the bottom wall of channel as shown in Figure 1 (a).

Considering the effect of rise in temperature of fluid in flow direction, the dynamic viscosity to be vary as follows (Incropera, 1999)

$$\mu(T) = 2.414 \times 10^{-5} \times 10^{(247.8/(T-140))}$$

where

- μ = Fluid dynamic viscosity
- T = Fluid temperature.

The variation in all other properties of the fluid are seen to be insignificant with temperature rise in fluid flow direction in the channel. Therefore they are treated to be constant.

Figure 2 indicates the meshing of CWMC. The grid independence test is carried out at coarse, medium and fine edge sizes. The Nu and friction factor variations are very small as the grid size is reduced from medium to fine. Therefore to reduce the computational time, medium edge size is selected in numerical investigation. Results from numerical study are coincide with experimental carried out by Chiam et al. (2016). Details of the grid independent test are given in Table 1.

Table 1. Summary of grid independent test

Grid type	element size(mm)	No. of nodes	No. of elements	Nu	Friction factor
Coarse	0.0375	447678	408064	9.3	0.01694
Medium	0.025	1466325	1377792	9.64	0.01362
Fine	0.01875	3423420	3266560	9.71	0.01158

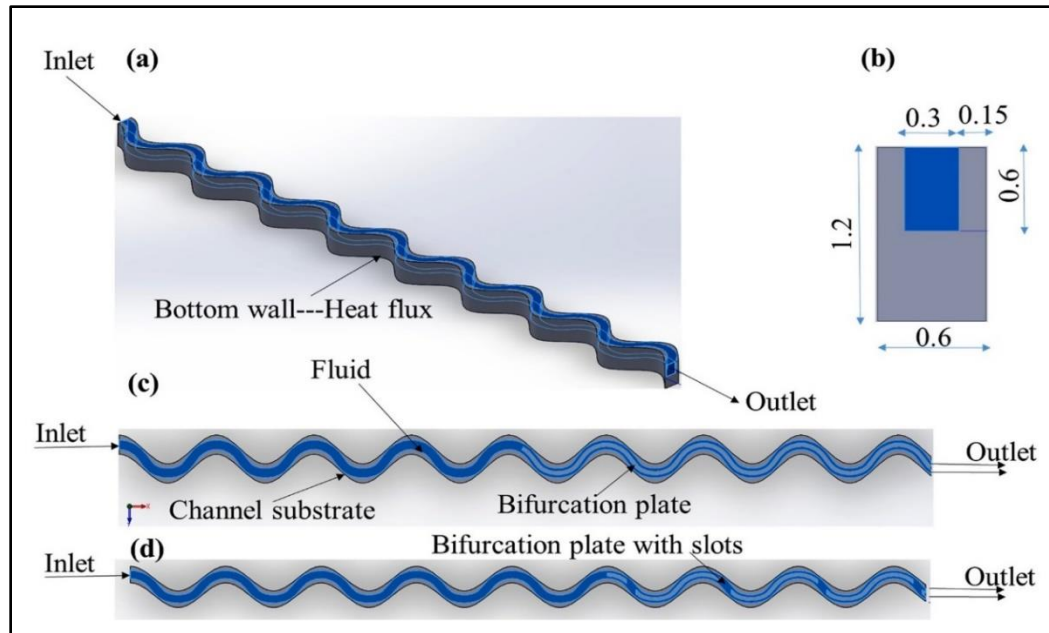


Figure 1. (a) CWMC with solid and fluid domain (b) cross section view of CWMC (c) CWMC with Bifurcation plate (d) CWMC Bifurcation plate with slots

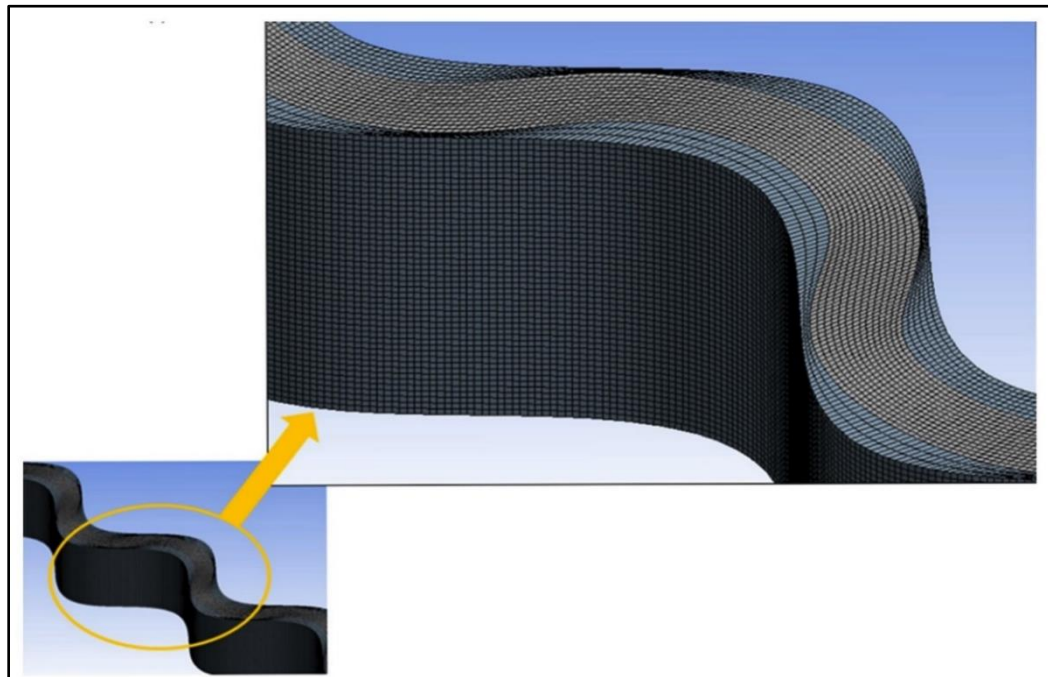


Figure 2. Meshing of CWMC

The governing equations for the current study as follows (Patankar, 1980):

Continuity equation,

$$\frac{\partial U}{\partial X} + \frac{\partial V}{\partial Y} + \frac{\partial W}{\partial Z} = 0 \quad (1)$$

X--Momentum equation,

$$U \frac{\partial U}{\partial X} + V \frac{\partial U}{\partial Y} + W \frac{\partial U}{\partial Z} = -\frac{\partial p}{\partial X} + \frac{1}{Re} \left(\frac{\partial^2 U}{\partial X^2} + \frac{\partial^2 U}{\partial Y^2} + \frac{\partial^2 U}{\partial Z^2} \right) \quad (2a)$$

Y-- Momentum equation,

$$U \frac{\partial V}{\partial X} + V \frac{\partial V}{\partial Y} + W \frac{\partial V}{\partial Z} = -\frac{\partial p}{\partial Y} + \frac{1}{Re} \left(\frac{\partial^2 V}{\partial X^2} + \frac{\partial^2 V}{\partial Y^2} + \frac{\partial^2 V}{\partial Z^2} \right) \quad (2b)$$

Z-- Momentum equation,

$$U \frac{\partial W}{\partial X} + V \frac{\partial W}{\partial Y} + W \frac{\partial W}{\partial Z} = -\frac{\partial p}{\partial Z} + \frac{1}{Re} \left(\frac{\partial^2 W}{\partial X^2} + \frac{\partial^2 W}{\partial Y^2} + \frac{\partial^2 W}{\partial Z^2} \right) \quad (2c)$$

Energy equation,

$$U \frac{\partial \theta}{\partial X} + V \frac{\partial \theta}{\partial Y} + W \frac{\partial \theta}{\partial Z} = \frac{1}{Re.P_r} \left(\frac{\partial^2 \theta}{\partial X^2} + \frac{\partial^2 \theta}{\partial Y^2} + \frac{\partial^2 \theta}{\partial Z^2} \right) \quad (3)$$

where, θ is dimensionless Temperature, $\frac{\partial p}{\partial X}$ is the pressure gradient and Re, P_r are Reynolds and Prandtl numbers respectively. In numerical simulation, fluid (water) domain is surrounded by channel substrate material (copper) with half thicknesses considered. The periodic boundary conditions are applied on both sides of channel walls. This to indicate that there are multiple channels on both sides. Hence this is free boundary condition. computational solution is converged once all the residues are reaches to 10^{-6} .

3. Data Reduction

(i) Hydraulic Diameter (D_h)

$$D_h = \frac{2HW}{(H+W)} \quad (4)$$

(ii) Reynolds Number(Re)

$$Re = \frac{\rho U_{in} D_h}{\mu} \quad (5)$$

(iii) Local Nusselt Number(Nu_x)

At steady state the heat energy entering into MC substrate must be equal to the heat energy exiting from the MC substrate.

$$q'' * A_b = q''_w * A_w \quad (6)$$

Local convective heat transfer coefficient h_x is determined using the below equation:

$$h_x = \frac{q''_w}{T_{w,x} - T_{f,x}} \quad (7)$$

The local Nusselt number is

$$Nux = \frac{h_x * D_h}{K_f} \quad (8)$$

Average Nusselt number is estimates as arithmetic mean of local Nusselt number at 25 isolations.

$$Nu_{avg} = \frac{\sum_{x=0}^{25} Nu_x}{25} \quad (9)$$

(iv) Friction Factor (f)

$$f = \frac{\frac{dP}{dx} D_h}{\frac{1}{2} \rho U_{in}^2} \quad (10)$$

(v) Performance Factor (P_f)

The performance of the MC heat sink is represented by performance factor (P_f), which depends on Nu and P_f . It is the ratio of Nu to the P_f . The performance factor as defined in (Chiam et al., 2016) for any given design (B) compared to a reference design (A) is given by

$$P_{fB} = \frac{\frac{Nu_B}{f_B}}{\frac{Nu_A}{f_A}} \quad (11)$$

where ‘A’ refers to reference design (SWMC) and ‘B’ refers to the present design that is compared with the reference.

4. Experimental Validation

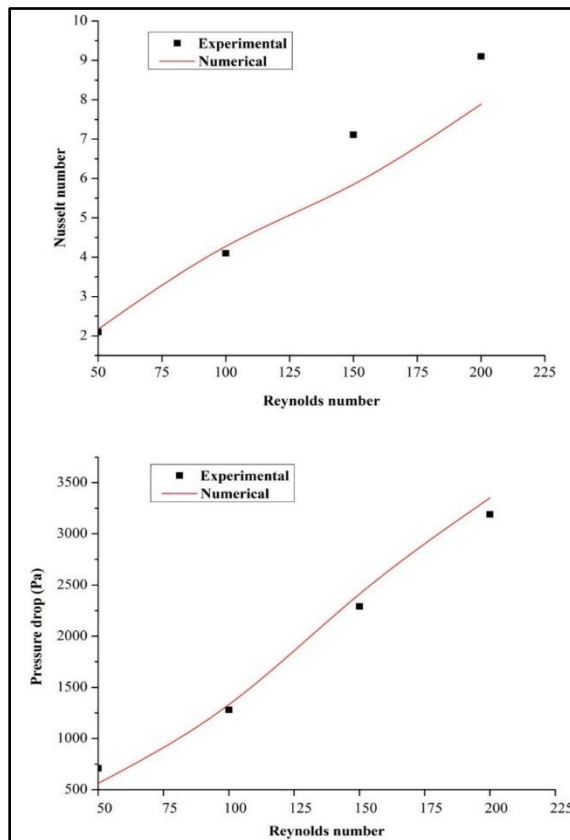


Figure 3. Comparison between experimental results (Chiam et al., 2016) and numerical results

The present numerical approach is validated with the experimental outcomes given in (Chiam et al., 2016). The test pieces in (Chiam et al., 2016) were made-up on copper with footprint of 25×25 mm. The test piece was insulated on all four sides. Water was the working fluid and the heating load of up to 1000W was supplied by 4 cartridge heaters. The calculations were based on uniform heat flux input. Considering the maximum heat input as 1000W and footprint area as 6.25 cm², the maximum possible heat flux would be 160 W/cm². Since the exact value of heat flux used for their experiment has not been reported, a safe assumption of 130 W/cm², well within limits, was taken where the numerical results from the current studies concurred well with corresponding experimental results. From Figure 3 it is observed that, experimental and numerical studies are in coincide with a deviation of 3% to 17% in Nu and 3% to 20% in pressure drop.

5. Results and Discussion

5.1. Span-Wise Velocity Vector Profiles and Stream-Wise Velocity Contours

From Figure 4, it is observed that CWMC has more Dean vortices than SWMC. These Dean vortices, transverse the high temperature fluid from channel base to top level and brings the low temperature fluid from the top level to channel base. In CWMC, formation of secondary vortices is also higher. This leads to an effective fluid mixing and subsequently enhances the heat transfer. From Figure 5, it is observed that the boundary layer in SWMC is thicker while boundary layer in CWMC is thinner. The boundary layer thickness further reduces in CWMC with BFP. As boundary layer thickness reduces, higher temperature difference between the MC substrate and fluid is observed. This leads to augmented convective heat transfer rate and subsequently increase in Nu. As the Re increases, the boundary layer thicknesses reduces further and consequently increases the Nu. As bifurcation plate (BFP) is introduced in the middle of the MC, it leads to further thinning of the boundary layer. This also promotes increase in heat transfer surface area and the formation of longitudinal vortices in addition to the Dean vortices. These formations are favourable to enhance the heat transfer. In CWMC with BFP, as slots are introduced in BFP, it leads to further thinning and re-initialization of boundary layer and hence augments the convective heat transfer.

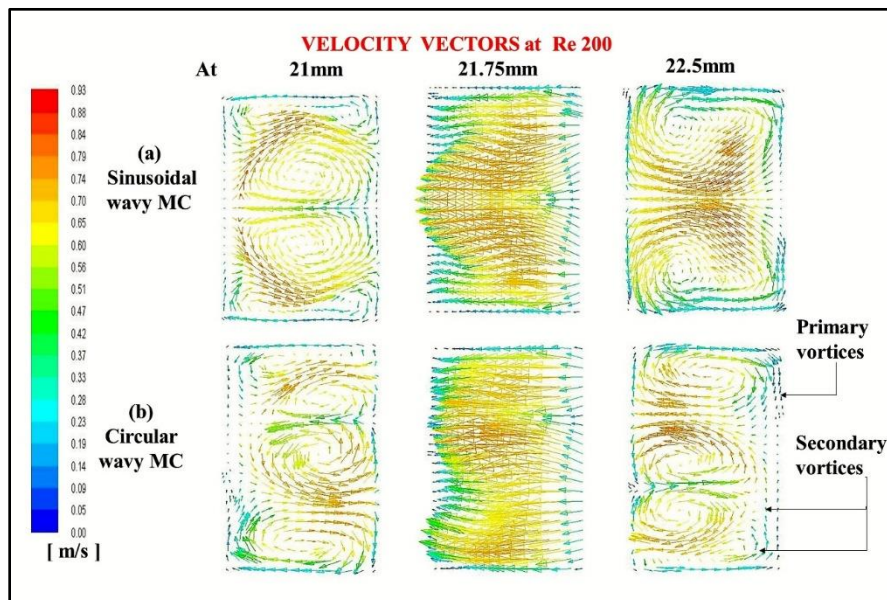


Figure 4. span-wise velocity vector profiles

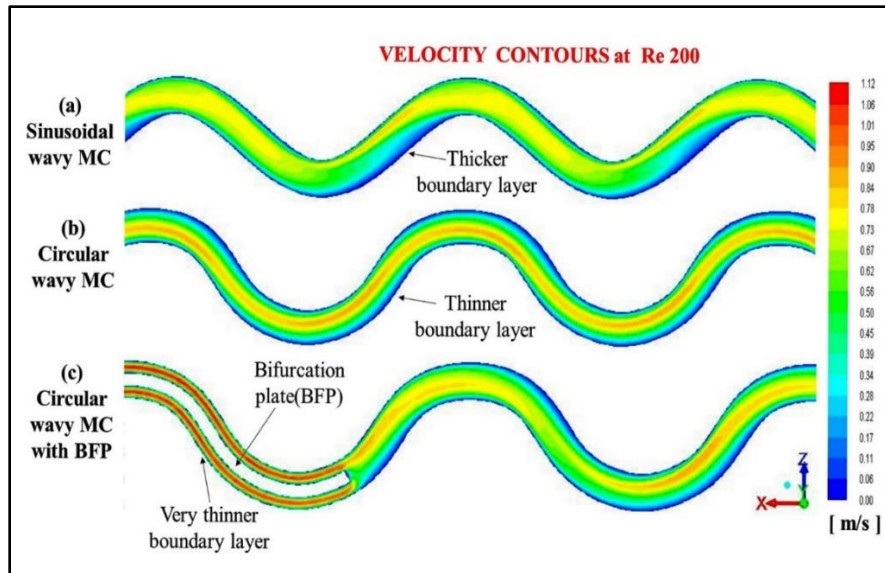


Figure 5. Stream-wise velocity contours at Re 200

5.2. Heat Transfer Enhancement

Figure 6 illustrates variation of Nu variation with Re for several designs considered in the current study. From Figure 6, it is observed that Nu enhancement has a positive relation with Re. CWMC has higher Nu than SWMC with smaller pressure drop penalty in the Re range of 100 to 300. This is due to the development of more Dean vortices in CWMC than SWMC. In SWMC, the radius of curvature of channel passage changes from crest to trough. It is smaller at crest and trough and larger between them. Hence in SWMC, Dean vortices at peak and trough are stronger and weaker between those two. In CWMC, radius of curvature of channel passage is constant. Hence, it has uniform Dean vortices strength. Dean vortices strength can be observed from Figure 4. CWMC with BFP and CWMC with BFP slots show higher heat transfer than SWMC and CWMC. The reasons are explained in previous section. From the numerical study, it is identified that the Nu enhancement in CWMC is 16.5%, in CWMC with BFP (7.5 mm, 10 mm and 12.5 mm) it is (64.8%, 85.4% and 90%) respectively and in CWMC with BFP (10 mm) with slots it is 109.2% higher than SWMC at Re 200.

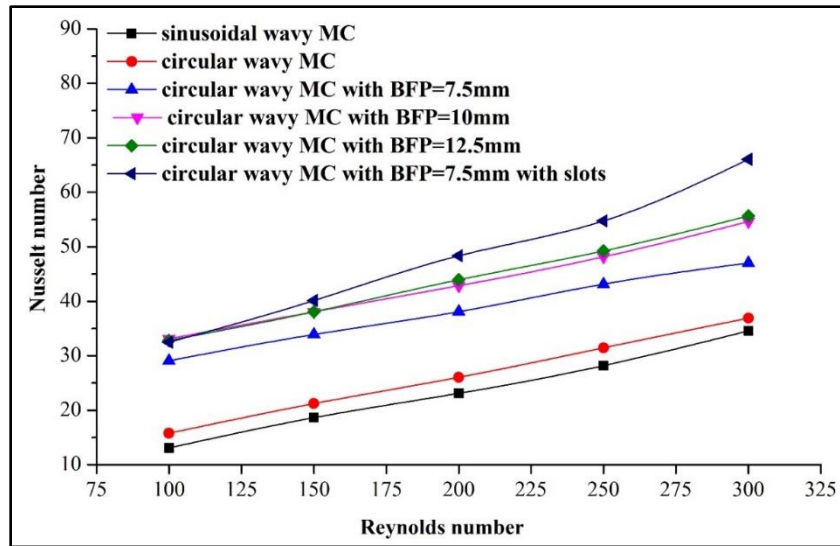


Figure 6. Nu vs. Re

5.3. Temperature Difference Between Channel Inner Surface and Fluid along Channel Length

From Figure 7, it is observed that temperature difference (between the channel inner surface and fluid) in SWMC is in cyclic variation whereas in CWMC, it is in linear variation. It is also observed that in CWMC, temperature difference is lower than SWMC. This is due to additional Dean vortices formation in CWMC. Due to this, fluid absorbs enormous heat from the channel substrate material and subsequently enhances heat transfer. In CWMC with BFP, the temperature difference is lower than SWMC and CWMC. Temperature difference is further reduced as BFP length increases. Similarly, CWMC (BFP=10 mm with slots) gives lowest temperature difference nearer the outlet. Reasons for this were explained in earlier section (Section 5.1).

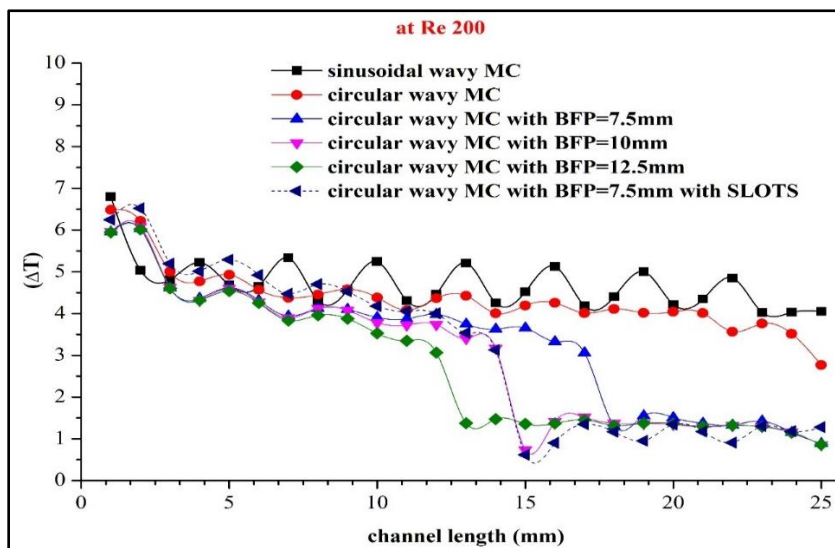


Figure 7. Temperature difference along the channel length at Re 200

5.4. Pressure Drop Penalty

From Figure 8 it is noticed that pressure drop penalty in CWMC is higher than in SWMC in the Re range considered in the present study. This is due to the fact that the fluid has to take a 180° turn while flowing through circular channel passage. This causes momentum losses and leads to higher pressure drop than SWMC. As bifurcation plate is introduced in the middle of CWMC channel passage, it restricts the fluid flow. Hence pressure drop penalty is higher than for SWMC and CWMC. As bifurcation plate length increases, pressure drop penalty increases further. For CWMC with BFP(10 mm) with slots, pressure drop is lower than for CWMC with BFP(10 mm) in Re range considered for the present study. This is because BFP with slots allows the fluid flow with smaller frictional resistance. From the present studies, it is noticed that pressure drop penalty in CWMC is 16.5 %, in CWMC with BFP(7.5 mm, 10 mm and 12.5 mm) it is 161.8%, 216.3% and 272.5% respectively and in CWMC with BFP(10 mm) with slots, it is 202.6% higher than SWMC at Re 200.

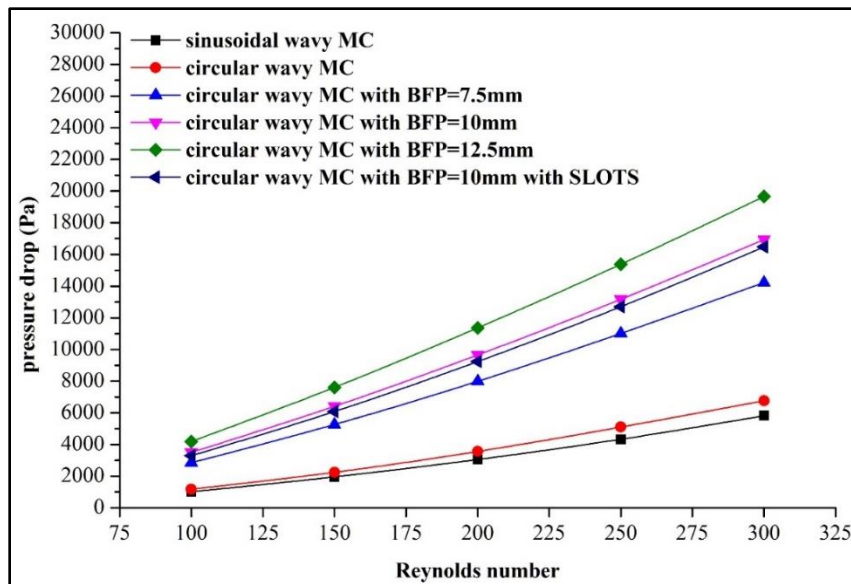


Figure 8. Pressure drop vs. Re

5.5. Performance Factor (P_f)

Figure 9 illustrates the variation P_f with Re. It is identified that for all the designs considered in present study, P_f decreases gradually as Re increases. It is because, the pressure drop penalty is predominant than heat transfer enhancement. In the present study, it is observed that CWMC has higher P_f , CWMC with BFP=12.5 mm has lower ' P_f ' and CWMC with BFP (10 mm) with slots has moderate P_f .

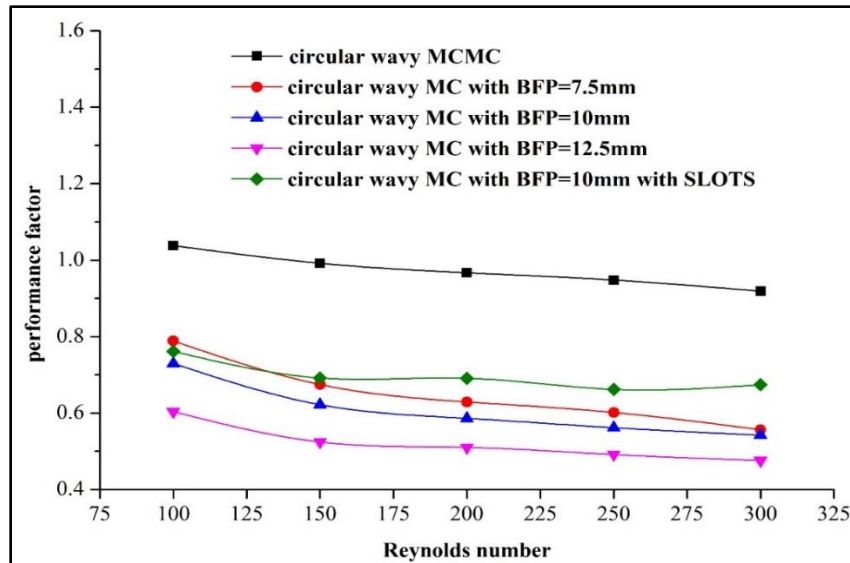


Figure 9. P_r vs. Re

6. Conclusion

Numerical simulation was conducted on CWMC and CWMC with BFP(with slots) and their results were compared with SWMC. The following are the concluding remarks from this numerical study.

- CWMC has higher Nu than SWMC with pressure drop penalty considered in Re range.
- CWMC with bifurcation plate provides higher Nu with an expense of pressure drop penalty.
- In CWMC, as bifurcation plate is introduced, temperature difference between fluid and channel inner surface is decreased along the flow direction.
- CWMC with bifurcation plate length of 10 mm with slots provides moderate performance factor.

Conflict of Interest

The authors confirm that this article contents have no conflict of interest.

Acknowledgement

This work was completed as a part of SERB (ECR/2016/000119), is gratefully acknowledged.

References

- Ambatipudi, K.K., & Rahman, M.M. (2000). Analysis of conjugate heat transfer in microchannel heat sinks. *Numerical Heat Transfer: Part A: Applications*, 37(7), 711-731.
- Chiam, Z.L., Lee, P.S., Singh, P.K., & Mou, N. (2016). Investigation of fluid flow and heat transfer in wavy micro-channels with alternating secondary branches. *International Journal of Heat and Mass Transfer*, 101, 1316–1330.

- Dean, W.R., & Hurst, J.M. (1959). Note on the motion of fluid in a curved pipe. *The London, Edinburgh, and Dublin Philosophical Magazine and Journal of Science*, 6(1), 77–85.
- Hasan, M.I., Rageb, A.A., Yaghoubi, M., & Homayoni, H. (2009). Influence of channel geometry on the performance of a counter flow microchannel heat exchanger. *International Journal of Thermal Sciences*, 48(8), 1607–1618.
- Incropera, F.P. (1999). *Liquid cooling of electronic devices by single-phase convection* (Vol. 3). New York: Wiley.
- Kandlikar, S.G., & Grande, W.J. (2004). Evaluation of single phase flow in microchannels for high heat flux chip cooling-thermohydraulic performance enhancement and fabrication technology. *Heat Transfer Engineering*, 25(8), 5–16.
- Karathanassis, I.K., Papanicolaou, E., Belessiotis, V., & Bergeles, G.C. (2013). Three-dimensional flow effects on forced convection heat transfer in a channel with stepwise-varying width. *International Journal of Thermal Sciences*, 67, 177–191.
- Knight, R.W., Hall, D.J., Goodling, J.S., & Jaeger, R.C. (1992). Heat sink optimization with application to microchannels. *IEEE Transactions on Components, Hybrids, and Manufacturing Technology*, 15(5), 832–842.
- Kumar, V.R., Balasubramanian, K., Kumar, K.K., Tiwari, N., & Bhatia, K. (2018). Numerical investigation of fluid flow and heat transfer characteristics in novel circular wavy microchannel. *Proceedings of the Institution of Mechanical Engineers, Part E: Journal of Process Mechanical Engineering*, DOI: 10.1177/0954408918820757.
- Kumar, V.R., Balasubramanian, K., Tiwari, N., Bhatia, K., & Kumar, K.K. (2019). Numerical investigation of heat transfer enhancement in wavy microchannel with tangential branched secondary channels. *Asia-Pacific Journal of Chemical Engineering*, DOI: 10.1002/apj.2325.
- Liu, D., & Garimella, S.V. (2004). Investigation of liquid flow in microchannels. *Journal of Thermophysics and Heat Transfer*, 18(1), 65–72.
- Patankar, S.V. (1980). *Numerical heat transfer and fluid flow*. Hemisphere. New York.
- Sui, Y., Teo, C.J., Lee, P.S., Chew, Y.T., & Shu, C. (2010). Fluid flow and heat transfer in wavy microchannels. *International Journal of Heat and Mass Transfer*, 53(13–14), 2760–2772.
- Tuckerman, D.B., & Pease, R.F.W. (1981). High-performance heat sinking for VLSI. *IEEE Electron Device Letters*, 2(5), 126–129.
- Xie, G., Shen, H., & Wang, C.C. (2015). Parametric study on thermal performance of microchannel heat sinks with internal vertical Y-shaped bifurcations. *International Journal of Heat and Mass Transfer*, 90, 948–958.

